Chapter 3

HIGHLY EFFICIENT AND BROADBAND HYBRID PHOTODETECTOR BASED ON 2D-GRAPHENE/CTS QUANTUM DOTS

This chapter includes the fabrication and characterization of Graphene/CTS QDs (2D/0D) based hybrid photodetection structure for broadband photodetection. The fabricated structure studied in this chapter improves the photodetection characteristics of stand alone CTS QDs based photoconductor structure as discussed in Chapter-2. The improvement in optical characteristics of hybrid structure results from the high mobility of CVD synthesized graphene which otherwise was low due to poor continuity of QDs films. On the other hand in comparison to only graphene based photodetector structures the fabricated structure shows sufficient improvement due to introduction of CTS QDs. This chapter also discuss the importance of fabricated graphene-CTS QDs based hybrid structure over other complex design broadband photodetectors *

*Parts of this chapter have been published in Sanjeev Mani Yadav, and Amritanshu Pandey. "Highly efficient and broadband hybrid photodetector based on 2-D layered Graphene/CTS quantum dots." *IEEE Transactions on Electron Devices* 66.8 (2019): 3417-3424.

3.1 Introduction

Broadband photodetectors (PDs) have wide range of application in solar cells, bio imaging, night vision cameras and optical communication [229, 230, 231] etc. Semiconductor materials for high sensitivity, high efficiency and fast response photodetectors in broad range are still a challenge. Hybrid systems are being explored so as the photo absorption and carrier movements are done separately to achieve fast speed and high sensitivity. Further, for broadband operation semiconductors with high bandgap tuning ability are required. Graphene is prominent material used for broadband photodetection due to its uniform light absorption across the optical spectrum, fast response time and ultra high carrier mobility [160, 232, 233, 161]. However, zero bandgap and very small absorption (∼2.3%) of light degrades the photoresponsivity of graphene [161, 94]. The methods used to improve the performance of graphene based PDs include creating hetero structures of it with some other low dimensional 2D materials (MoS_2 and WSe_2) [234, 235, 236], 1D nanowires (InAs and InSb) [237, 238], and 0D quantum dots (PbS, CdS, HgTe, and Cu(In,Ga)Se_2) [239, 240, 241, 242, 243]. The 2D materials have good absorption coefficient and cover large band gap (1–2 eV) but have low mobility and relatively longer relaxation time of carriers in compare to graphene therefore, the PDs made of these semiconductors are slow [244, 245, 246, 247]. While 1D materials show fast response and have good absorption coefficients, but their synthesis process is much more complex. Quantum dots (QDs) are most suitable owing to large absorption and their ability of large spectral range coverage due to size variations resulting from bandgap confinement effect. However, the toxicity of Hg, Cd, and Pb [248, 249, 250], as well as scarcity and high cost of materials such as Te, In, and Ga [251, 252] have prompted the search for better materials for PDs.

Cu_2SnS_3 (CTS) is a p-type semiconductor having large absorption coefficient (10000 cm^{-1}) and large bandgap tunability (0.93—-1.77 eV) [253, 254, 255]. It is earth-abundant, non-toxic and inexpensive element. The large surface to volume ratio of CTS QDs and large bandgap confinement effects make it suitable candidate for broadband PDs. Hybrid systems comprised of CTS QDs and high mobility graphene may

result in broadband, highly sensitive, and efficient PDs. The low cost solvothermal synthesis of CTS QDs leads to easy and cheap fabrication of photodetectors. In the present work, we report the fabrication and characterization of solvothermal synthesized CTS QDs and CVD grown mono layer/few layers graphene hybrid photodetector on SiO_2/Si substrate. The SiO_2/Si substrate provide the flexibility of integration with existing CMOS systems and the good optical contrast for optical inspection [256] of single layer or few layers graphene at microscopic scale. The resultant PD has wideband (vis-NIR), good responsivity ($\sim$110.089 A/W) and detectivity ($\sim 1.25 \times 10^{12}$ (cm $\cdot Hz^{1/2} \cdot W^{-1}$)). The resultant device outperforms the available closest devices based on CTS and graphene [255, 257, 258, 259].

3.2 Experimental Details

3.2.1 Solvothermal Synthesis of CTS Quantum Dots

A cationic solution of 0.3 mmol of $SnCl_2.2H_2O$ and 0.62 mmol of $CuCl_2.2H_2O$ was prepared in 20 mL of ethylene glycol followed by the addition of 1.6 M PVP (M_w = 2.5 g mol^{-1}). Here PVP is acting as a capping agent, preventing excessive growth and agglomeration, thus leading to the formation of CTS QDs. A another solution of 0.93 mmol of of Na_2S was prepared in 20 mL of ethylene glycol followed by ultrasonication for 5 min at room temperature (27 ^oC) to dissolve Na_2S in ethylene glycol as described in literature [255]. The resultant ultrasonicate solution was now added drop wise to cationic solution with magnetic stirring at room temperature with 500 r.p.m. The resultant brownish black solution was transferred to a 50 mL autoclave and kept at 180 ^oC for $\sim$12 h. The resultant product was now centrifuged and washed with ethanol and then vacuum-dried for 6 h at 80 ^oC. All the chemicals used were purchased from Sigma Aldrich, India and used as it is without any additional purification.

3.2.2 Chemical Vapor Deposition (CVD) Synthesis of Graphene

Mono/few layers of graphene films were grown on 25 μm thick Cu foil by the CVD technique using n-hexane as a liquid precursor[260]. An schematic of CVD setup along with experimental CVD setup have shown in Fig.3.1 and Fig.3.2 respectively. Cu foils were first loaded into quartz tube and then pumped down to 10^{-2} Torr using rotary pump to remove the trace gases present in it. Further the pressure of the quartz tube is maintained ~8-9 Torr for Ar/H_2 flow. The Temperature of the furnace was raised to 980^oC in the presence of H_2 ambient (with flow rate of ~400 sccm). As the desired temperature reached, the flow of H_2 gas was stopped and n-hexane vapour (flow rate ~4 mL/h) as carbon precursor was injected in the quartz tube for 4 minutes with the tube pressure of 500 mTorr. Further, furnace was cooled down to room temperature in H_2 atmosphere.

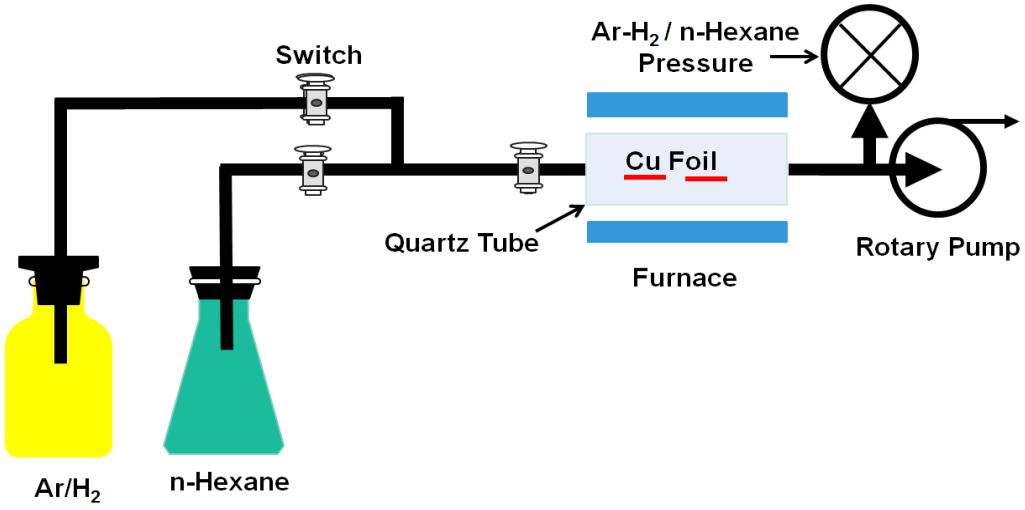

Figure 3.1: Schematic of CVD setup for growing graphene films

CVD synthesis of layered materials like graphene are having following advantages over other available synthesis techniques of 2D-materials [261].

- Offer high quality crystal synthesis with minimum defects.
- Large area synthesis
- Well control thickness (mono to few layers synthesis)

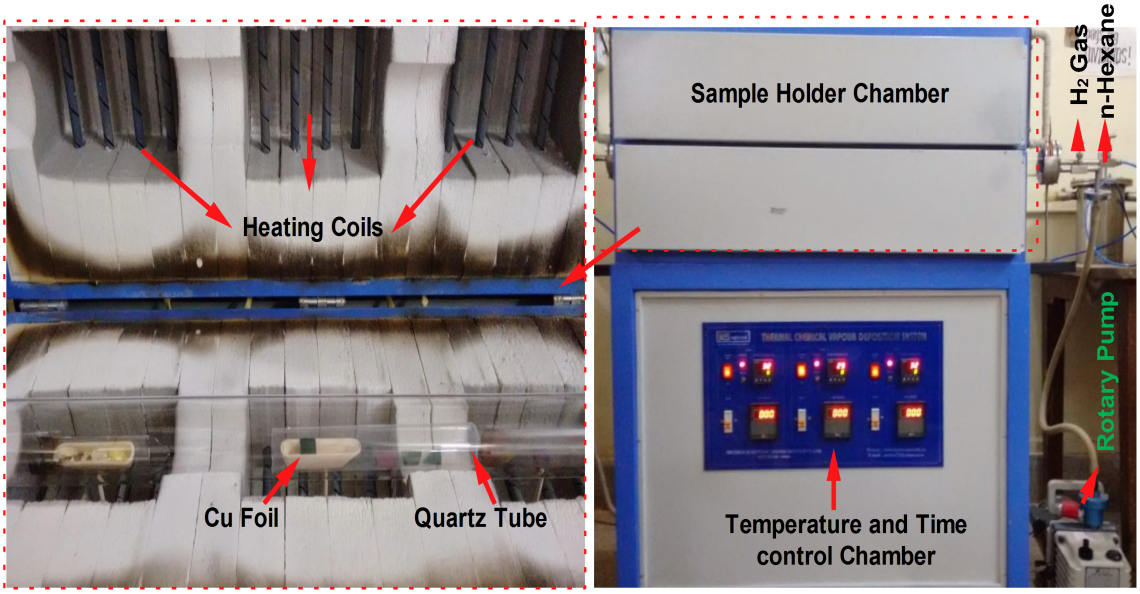

Figure 3.2: Experimental CVD setup used to synthesized mono or few layers of graphene

- Contamination free growth
- Uniformity in synthesized materials

3.2.3 Device Fabrication

3.2.3.1 Substrate Cleaning

The boron doped p-Si (100) substrates (resistivity $\sim$ 2–7 ohm-cm) were first cleaned in trichloroethylene through ultrasonic for 5 min. Then the wafer was dipped into the acetone solution for 5 min. After rinsing in DI water, it was dipped in H_2O_2 and H_2SO_4 (ratio of 60:40) solution. After rinsing again with the DI water, it was dipped in the solution of DI water and HF of ratio 6:1 for 5 min. In final step the wafer was rinsed through the running DI water.

3.2.3.2 Preparation of Oxide Layer on Silicon Substrate

After cleaning the Si wafer, it was immediately loaded into the quartz tubular furnace. Temperature of the furnace was set at 1000 ^{o}C. For the growth of 300 nm oxide layer we first performed dry oxidation for 15 min followed by wet oxidation for 30 min after

that again dry oxidation for 15 min was performed.

3.2.3.3 Transferring Graphene on SiO_2/Si Substrate

Graphene grown on Cu foil was transferred on SiO_2/Si substrate using wet polymer transfer method discussed in [260] and also shown in Fig.3.3. First, a thin layer of Poly(methyl methacrylate) (PMMA) polymer is spin coated on Graphene/Cu foil, then Cu from the bottom is etched out in diluted nitric acid solution. After dissolving Cu foil, PMMA supported graphene is cleaned using DI water to remove the impurities. In the final step graphene floating with PMMA is fished out on SiO_2/Si substrate and PMMA was removed in acetone.

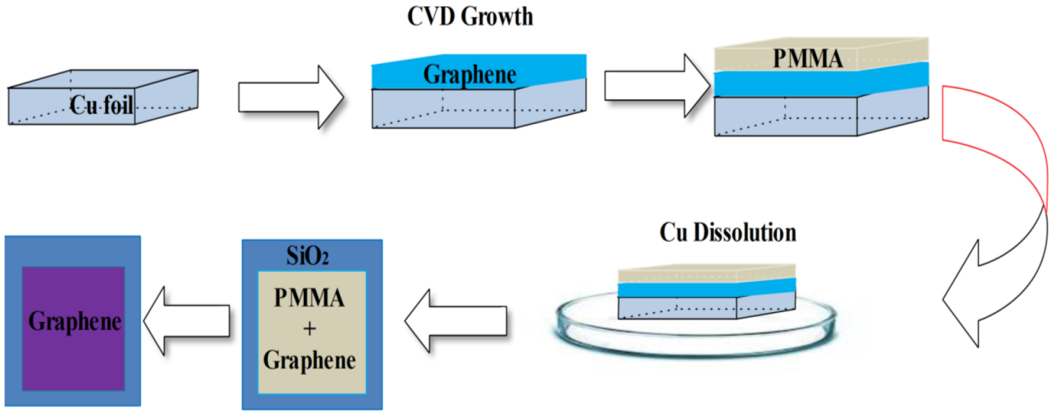

Figure 3.3: Transferring of CVD grown graphene on SiO_2/Si substrate by using wet polymer methods

3.2.3.4 Hybrid Structure of CTS-QDs/Graphene on SiO_2/Si Substrate

Square shape (2×2 mm^2 area) electrical contacts of Ag (∼90 nm thickness) were made on Graphene/SiO_2/Si structure through thermal evaporation (Vacuum Coating Unit Model-BC-300) of high purity Ag (99.99%) with shadow mask technique. After that 0.23 mg of synthesized CTS QDs dispersed in 1 mL ethanol was spin coated on Ag/Graphene/ SiO_2/Si structure at 500 r.p.m. for 1 min. The spin coating was repeated for three times. Finally, the resultant device was heated on hot plate at 40 ^oC for 5 min. The device schematic and fabricated device structure are shown in Fig.3.4 (a) and

(b) respectively.

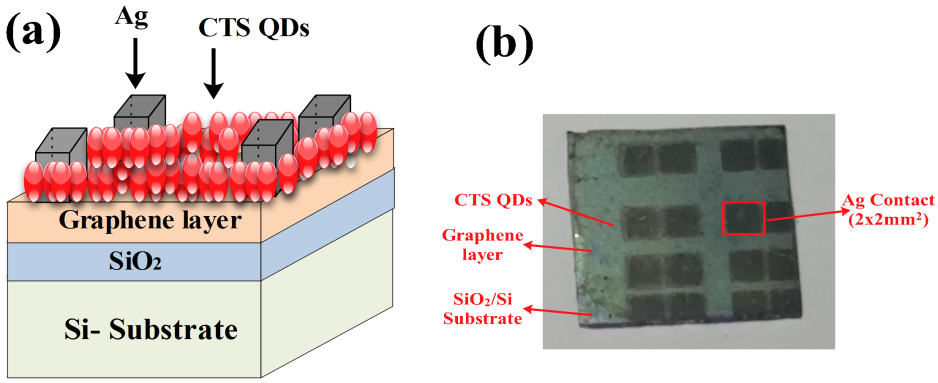

Figure 3.4: (a) Complete device schematic of CTS QDs/Graphene/SiO_2/Si based photodetector and (b) Fabricated device under consideration.

3.3 Results and Discussion

3.3.1 Structural Characterizations of Solvothermal Synthesized CTS-QDs and CVD Grown Graphene

3.3.1.1 Characterizations of Solvothermal Synthesized CTS-QDs

X-ray diffraction (XRD) analysis of solvothermal synthesized CTS QDs performed by Rigaku, Smartlab 9 kW powder type equipped with a Cu kα source of 1.5405 Å wavelength is shown in Fig.3.5. The XRD pattern of CTS QDs shows peaks at 28.10, 32.22, 34, 46.12, 48.60, 52.60, 56.81, 59.70, and 75.91 2θ angles which are identified to be reflection from (112), (200), (004), (204), (220), (301), (312), (224), and (332) planes of tetragonal CTS, respectively. The 2θ angles and their corresponding planes are found to match well with standard file for tetragonal CTS structure (JCPDS file no.: 089-4714). The major peaks of XRD pattern of CTS QDs are observed at 32.22 and 46.12 for 2θ angles which confirm the highly crystalline plane of CTS QDs for (200) and (204) orientation. However, the broadening of peak in the XRD pattern of CTS QDs signify the Smaller crystalline size, an inhomogeneous composition in a solution, stacking faults,

micro strain, and other defects in the crystal structure [262] etc.

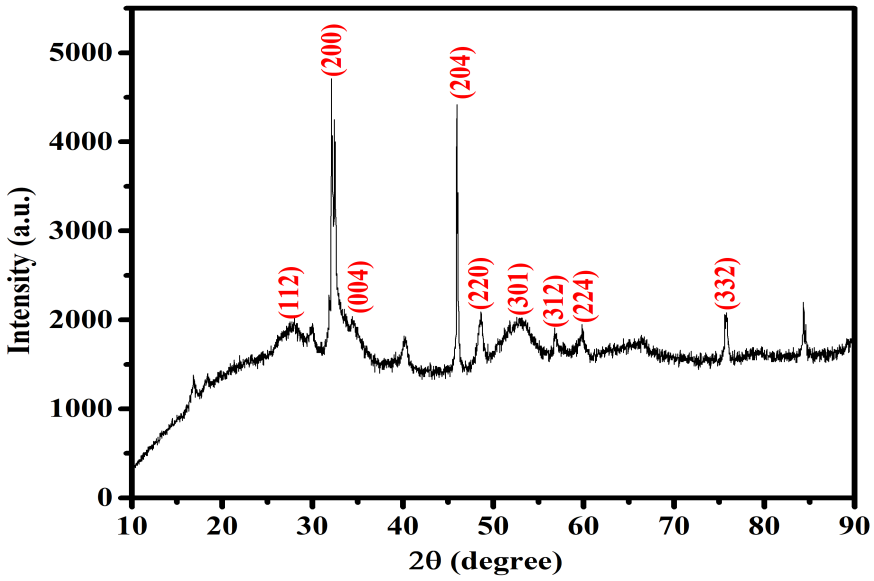

Figure 3.5: X-ray diffraction pattern of the CTS QDs

The Transmission electron microscopy (TEM), high resolution TEM (HR-TEM), selected area diffraction pattern (SAED) and fast Fourier transform (FFT) studies of CTS QDs were performed using Tecnai G2 20 Twin of FEI, USA. TEM image (Fig.3.6 (a)) confirms the formation of uniform size of CTS QDs with average size ∼3.7 nm which is less than the Bohr radius for CTS and hence can lead to quantum confinement [263]. In the inset quantum size variation w.r.t. the number is presented. Fig.3.6 (b) shows the TEM image of CTS QDs (marked as circle) at 20 nm scale. The HR-TEM image (Fig.3.6 (c)) of CTS QDs confirms the various crystalline planes and their interplanar distances. The HR-TEM corresponding SAED pattern of CTS QDs with inter planar spacing and FFT are presented in Fig.3.6 (d) and Fig.3.6 (e), respectively.

The absorption spectra (PerkinElmer, Lambda 25 UV/Vis Spectrometer) of CTS QDs as shown in Fig.3.7 (a) indicate near infrared region activity. The linear Tauc plot ((hv) vs $(\alpha hv)^{1/2}$) as shown in Fig.3.7 (b) confirm the indirect bandgap nature having bandgap ∼1.32 eV of CTS QDs. The band gap of our synthesized CTS QDs is higher than that of CTS thin film [258] and lower than that of CTS QDs reported in [255].

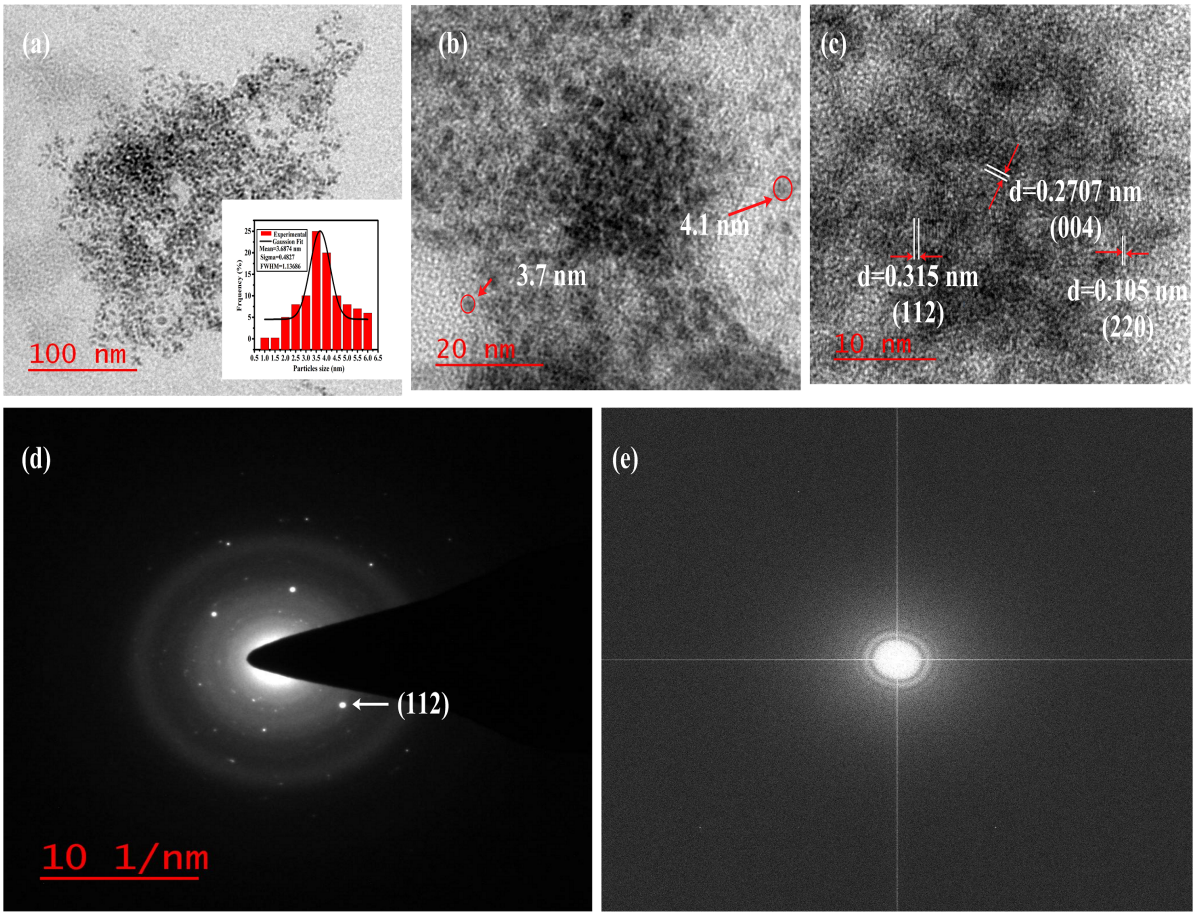

Figure 3.6: (a) TEM micrograph showing highly dispersed CTS- QDs with frequency (occurrence) of particle vs particles size plot inset, (b) TEM image of CTS QDs at 20 nm scale with circled CTS QDs, (c) HR-TEM image of CTS QDs with marked interplanar spacing and plane indexing, (d) SAED pattern of CTS QDs with plane indexing, (e) FFT of HR-TEM.

The indirect bandgap may be attributed to either localized state in band gap or defects or amorphous nature of synthesized CTS QDs [264].

The cyclic voltammetry (Autolab (PGSTAT) 101, Metrohm, Netherlands) measurement was also performed to find out the bandgap of synthesized CTS QDs. The three electrode measurement included Ag/AgCl reference electrode, Pt as a counter electrode and glassy carbon as working electrode. The electrodes were placed in KOH (0.1 M) in DI water electrolyte, while QDs sample were drop-casted on glassy carbon electrode for measurement while the voltage scan rate was kept 0.1 V/s. The cyclic voltammetry scan (Fig.3.8) of CTS QDs between -0.2 V to 1.6 V is used to calculate the bandgap of the synthesized QDs [255] and it is found to be ∼1.24 eV. Both the methods of

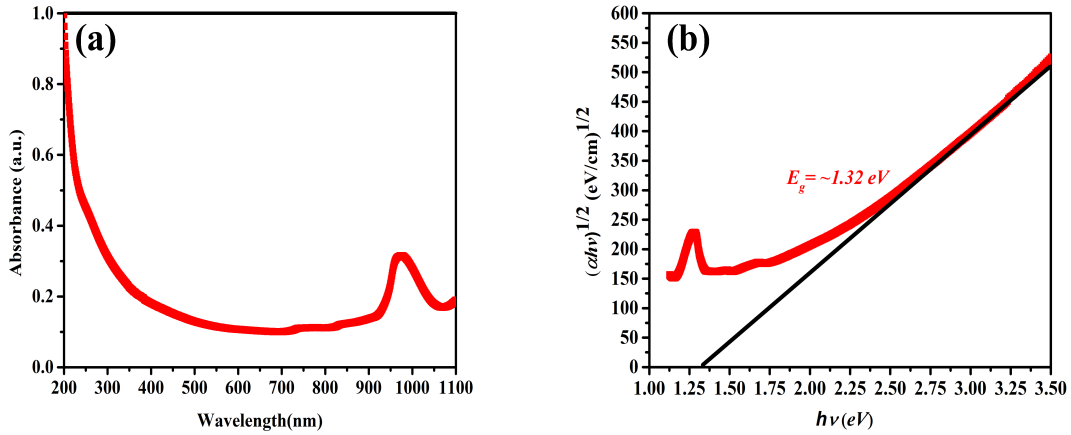

Figure 3.7: (a) Absorption spectra of CTS QDs, (b) Tauc-plot to estimate band gap

bandgap calculation are having close result (difference ∼0.08 eV) and confirm the NIR band operation of CTS QDs.

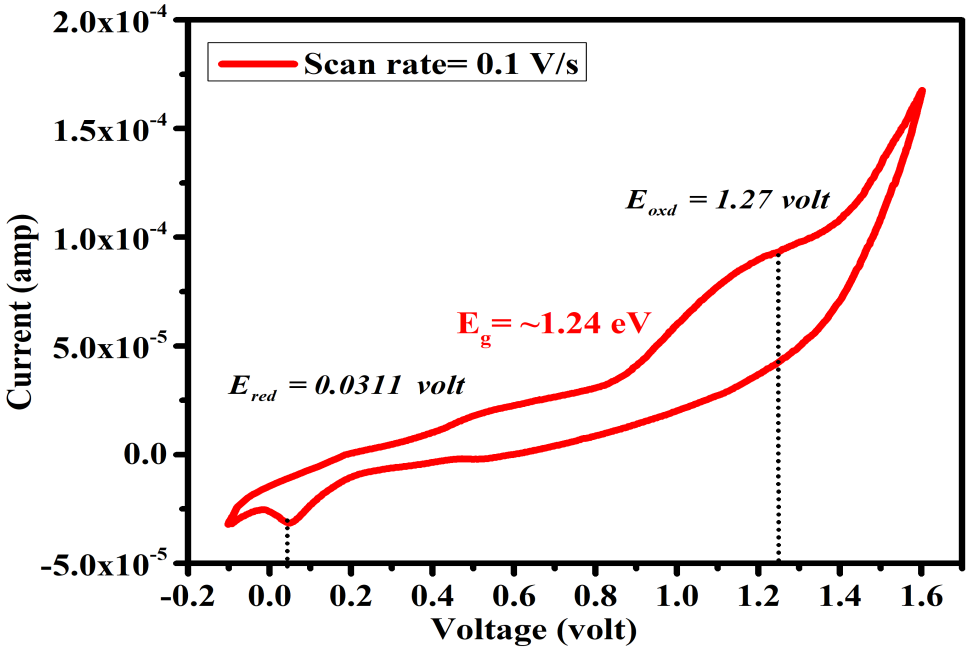

Figure 3.8: Cyclic voltammetry of the CTS QDs sample

3.3.1.2 Characterizations of CVD Grown Graphene

The transmission electron morphology of CVD grown graphene on Cu grid is shown in Fig.3.9 (a). The TEM image of CVD grown graphene presented large continuity with less wrinkle and defects over larger area. TEM data also confirm the growth of monolayer graphene at larger area in comparison to few layers of graphene. Raman spectra of CVD grown graphene were recorded using Raman Spectroscope (Renishaw inVia, Germany) with a laser excitation of 532 nm. In the Raman spectra of graphene (Fig.3.9 (b)) three peaks are observed at 1350, 1580 and 2700 cm^{-1}, which correspond to the D, G and 2D bands of graphene [260]. In most of the region of graphene film it has been observed that intensity ratio of 2D and G bands were higher that 2, which corresponds to the single layer graphene. In some region the intensity ratio was less than 1, which corresponds to the multi-layer graphene. So, Raman analysis also reveals the presence of single layer graphene film having some multi-layer islands over it.

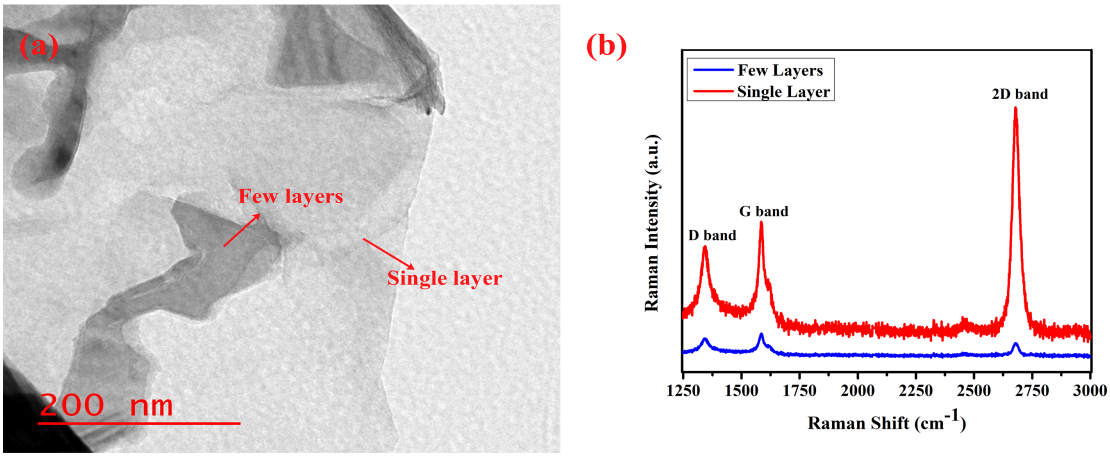

Figure 3.9: (a) TEM micrographs showing single layer graphene (darker region) having some multilayer islands (darker region) over it, (b) Raman spectra of single/few layers graphene film grown by CVD technique

3.3.1.3 Composite Characterizations of CTS-QDs and CVD Grown Graphene

The Field-emission Scanning Electron Microscope (FE-SEM) image of CTS QDs on Graphene/SiO_2/Si substrate at 10 μm scale are shown in Fig.3.10 (a). The Strong

agglomeration of CTS QDs with various sizes are observed which confirm the broadband detection of light. Fig.3.10 (b) show the FE-SEM image of CTS QDs coated on Graphene/SiO_2/Si substrate layer at 200 nm scale. Fig.3.10 (d) shows the energy-dispersive X-ray spectroscopy (EDS) of selected area in FE-SEM image marked in Fig.3.10 (c). The EDS of marked spot confirms the presence of elements (i.e Cu, Sn, S) which were used to synthesized the CTS QDs.

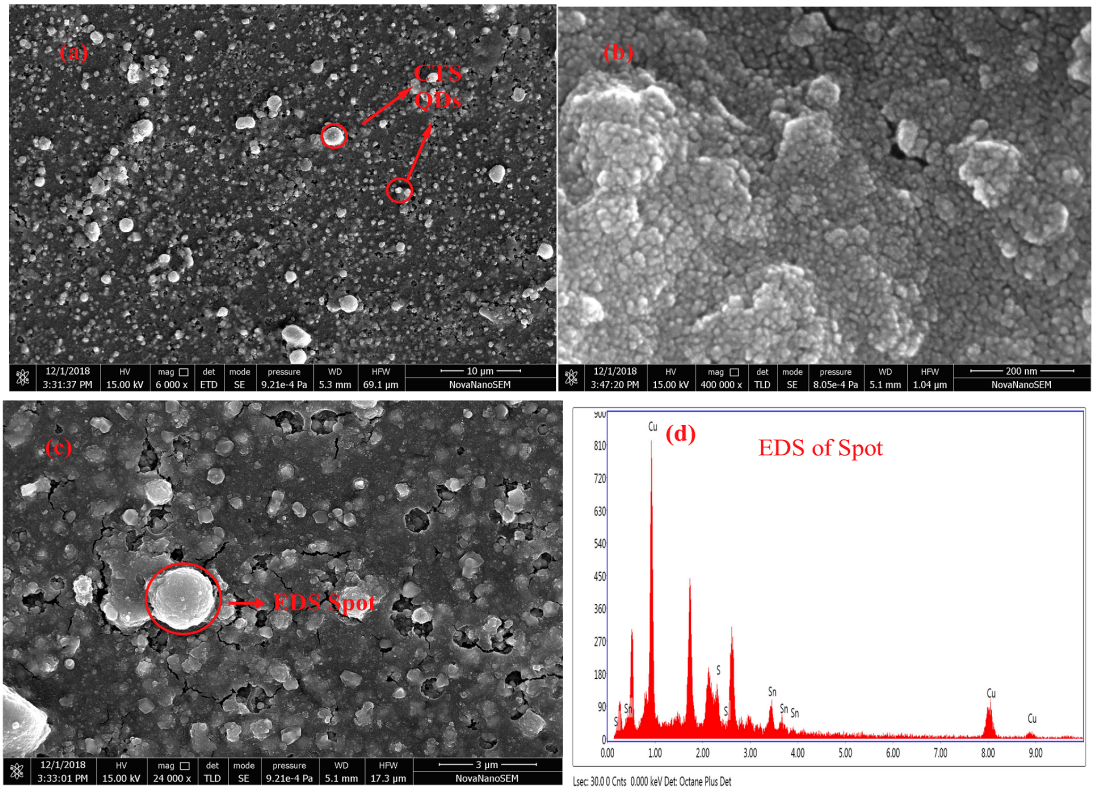

Figure 3.10: (a) FE-SEM image of CTS QDs on Graphene/SiO_2/Si substrate at 10 μm scale, (b) SEM image of the thin layer of agglomerated CTS-QDs dispersed over Graphene/SiO_2/Si substrate at 200 nm scale, (c) FE-SEM image of CTS QDs with marked spot, (d) The EDS of marked spot in (c)

3.3.2 Electrical and Optical Characterization

The current density-voltage ($J-V$) characteristics of CTS QDs/Graphene/SiO_2/Si based photodetector for broadband light detection are performed by parameter analyzer (Keysight, B1500A) under dark and illuminated conditions (Fig.3.11). The Monochro-

mator and Light Source (Princeton Instruments) having wavelength dependent power profile was used to illuminate the device at wavelengths of 650, 750, 850, and 1066 nm with optical power density 202.32, 175.79, 108.43, and 123.087 (μW/cm^2), respectively (Measured by calibrated Thorlabs PM100D power meter).The incident optical power is absorbed by the CTS QDs and in result photocarriers are generated. Hence, an enhanced current is obtained after illumination. The significant ratio of illuminated to dark for these wavelengths of device potentially leads our device a broadband (vis-NIR) photodetector, having better sensitivity for forward as well as for reverse bias as comparison to the devices based on CTS [258, 265] and graphene [266]. The photon to dark current ratio for 650, 750, 850, and 1066 nm wavelengths at 4.5 V were found to ∼7.19, ∼7.26, ∼7.32, and ∼7.29, respectively. The CTS QDs size variation is manifested in multiple bandgap CTS QDs ($E_g \sim 1/R^2$, R is radius of QDs), and the resultant device is almost equally sensitive in the broadband covered. Larger bandgap tunability of CTS QDs motivated us for its application in broadband photodetection in conjunction with high mobility graphene to achieve outstanding characteristics such as high responsivity, high detectivity and fast response time.

The spectral response analysis (current-wavelength, responsivity and detectivity) were carried out using monochromator (Princeton Instruments, SP2150i) and digital multimeter (Agilent, 34410A) at a scan rate of 60 nm/min. The larger current density for vis-NIR illumination justify the high absorption of light by CTS QDs for this region. Further, the photo current density of the detector is the function of applied voltage and vary significantly as the voltage changes from 2.5 to 4.5 V. Fig.3.12 (a) and (b) show the current density variation for different wavelengths at two bias 2.5 V and 4.5 V, suggesting vis-NIR band operation. The responsivity (R) of the device is measured as the electrical output per incident optical input, while the EQE of the device defines the ratio of photo electrons produced by the incident light to the numbers of incident photons. The calculation of EQE along with R, has also been performed for measuring optical to electrical conversion efficiency of the detector.

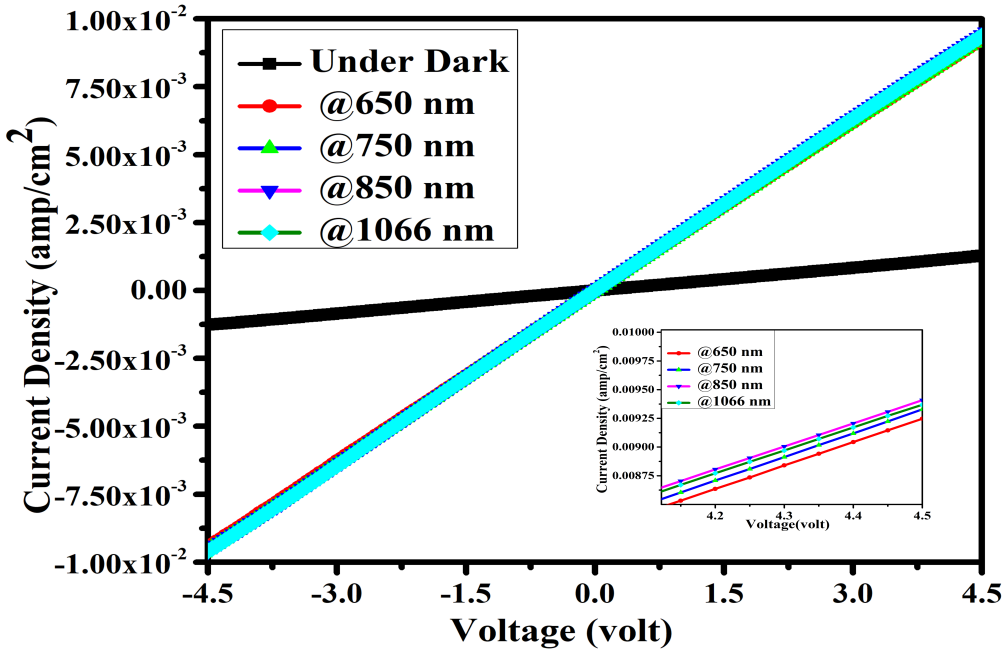

Figure 3.11: J-V characteristics of CTS QDs/Graphene/SiO_2/Si based photodetector at different wavelengths with magnification scale plot inset

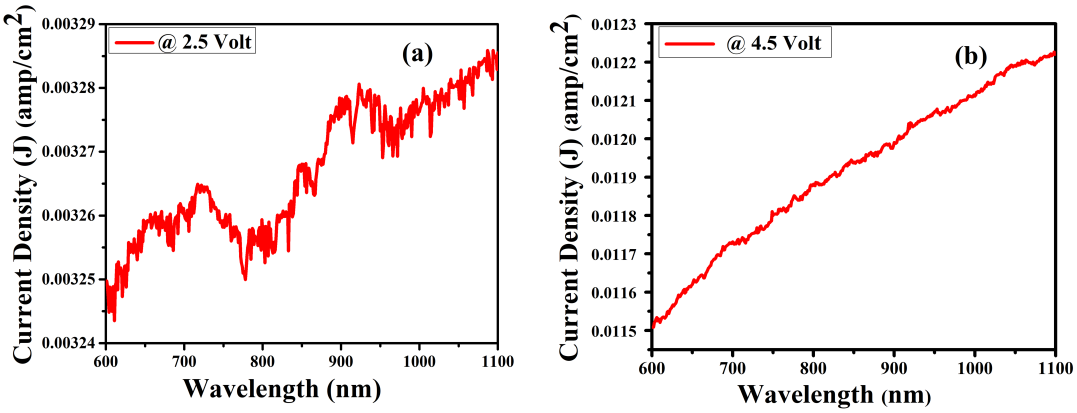

Figure 3.12: (a) Photo current density vs wavelength characteristics of CTS QDs/Graphene based photodetector at 2.5 V and, (b) at 4.5 V

The responsivity of photodetector is calculated by using relation

$$Responsivity(R) = \frac{J_p}{P_{opt}} \tag{3.1}$$

Where J_p is the photo current density and P_{opt} is illuminated power density. Detectivity is defined as

$$Detectivity(D) = \frac{\lambda \eta q}{hc}\sqrt{\frac{RA}{4kT}} \tag{3.2}$$

Here RA is the resistance area product. RA is defined as

$$\left(\frac{\partial J}{\partial V}\right)^{-1} = \frac{kT}{qJ} = RA \tag{3.3}$$

The Responsivity (Fig.3.13 (a)) and Detectivity (Fig.3.13 (b)) of the proposed CTS QDs/graphene based photodetector (at 2.5 V and 4.5 V) are found better than the reported CTS and graphene based photodetectors [257, 258, 255, 259, 241]. The best responsivity, detectivity and quantum efficiency is found 110.089 (A/W), 1.25×10^{12} (cm $\cdot Hz^{1/2}$ $\cdot W^{-1}$), and 160.90, respectively at 4.5 V bias under 850 nm illumination.

The time response of CTS QDs/Graphene/SiO_2/Si based photodetector, performed at 4.5 V under vis-NIR lamp (Murphy Infrared, 150 W) is shown in Fig.3.13 (c). The spectral response of vis-NIR lamp, measured by spectrometer (UCB 2000, Ocean Optics) confirms that major portion of light wavelengths falls in vis-NIR region. This vis-NIR lamp was switched ON and OFF manually for 15 s to measure the time response of our photodetector. The ON and OFF time of CTS QDs/Graphene/SiO_2/Si based photodetector found to be 10.2 and 11.34 s respectively which is generally comparable with CTS based photodetector discussed in literature [257, 258] and Graphene based photodetector [241], despite of being many times larger in scale. So this chapter report fabrication of high responsivity, detectivity and quantum efficiency based photodetector for broad spectral ranges with less response time.

Fig.3.13 (d) shows the $C-V$ response of device under dark and vis-NIR lamp illumination at 1 MHz. The increased capacitance for all bias voltages under vis-NIR illumination with respect to dark condition clearly indicates the reduction in the overall depletion width of photodetector. The increased capacitance increases the potential energy *(E=0.5CV ^{2})* stored in the junction capacitance which consequences the CTS QDs/Graphene-based photodetector to work at lower bias voltage [267] and reduce the dark current [268].

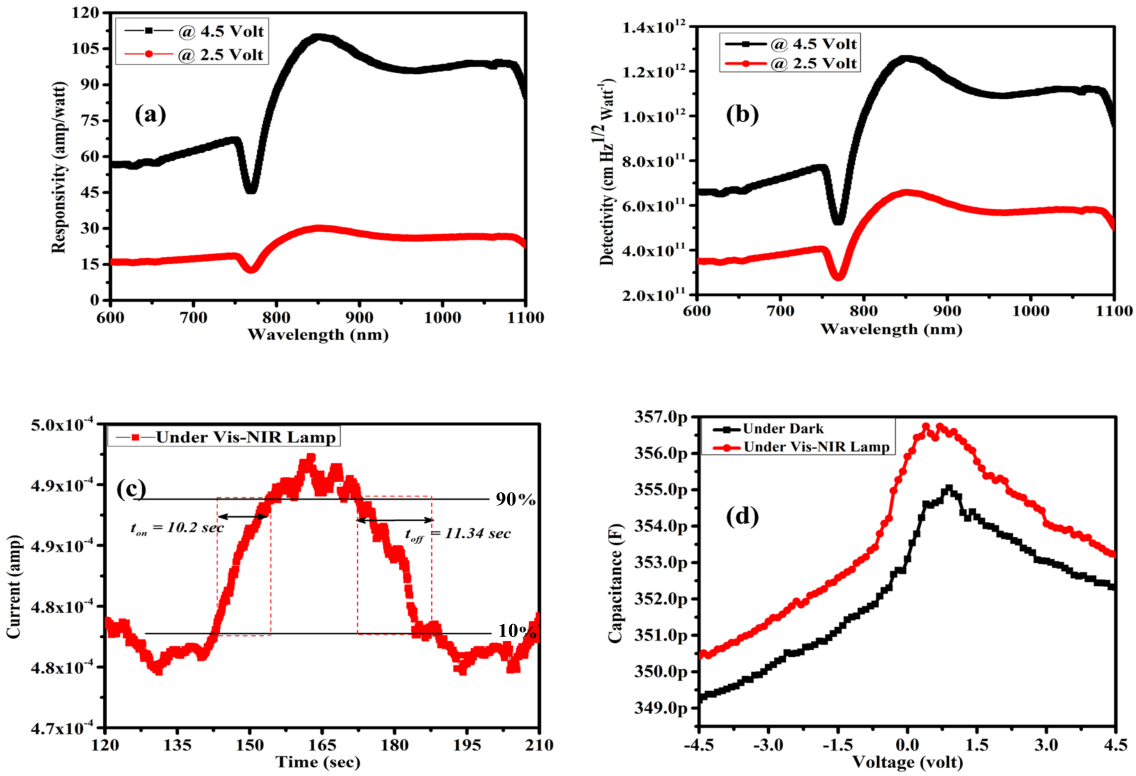

Figure 3.13: (a) Responsivity vs wavelength, (b) Detectivity vs wavelength plot of CTS QDs-Graphene based photodetector under vis-NIR light illumination, (c) Time response under Vis-NIR illumination and, (d) C-V response under dark and Vis-NIR illumination

In comparison to other photodetectors [255, 257, 258, 259, 241] our detectors are showing high responsivity, detectivity, EQE and accepted time response for lower optical power intensity as shown in Table-3.1.

The carrier transport of the proposed photodetector is expected to have following three components:

1. Ag-Graphene-Ag
2. Ag- CTS QDs-Ag
3. Ag-CTS QDs-Graphene-Ag

Ag-Graphene-Ag transport will have very little contribution in the overall photo current due to small absorption of light in graphene (i.e., less photo generated carriers)

Table 3.1: Comparison Among Other Reported CTS QDs and Graphene Based Broadband Photodetectors.

Parameters	**This work**	**[255]**	**[257]**	**[258]**	**[259]**	**[241]**
Device structure	Ag/CTS QDs/Graphene	Ag/CTS QDs/ITO glass	Ag/CTS QDs/ITO glass	Ag/CTS thin-film	Graphene/Si/ Graphene	Au/PbS QDs/ Graphene
Applied Bais (V)	4.5 V	.....	0V,-0.5V	3V	——–	4.5V
Wavelength (nm)	600–1100	1064 and 1550	1064 and 1550	880,920,1050	1300, 2100	895
Illumination Intensity (μW/cm^2)	108.43 (@ 850 nm) 202.32 (@ 650 nm) 123.087 (@ 1066 nm)	50000 (@ 1064 nm)	550000 (@ 1064 nm)	——	——	32700 (@ 895 nm)
Responsivity (A/W)	110.089 (@ 850 nm) 57.43 (@ 650 nm) 99.124 (@ 1066 nm)	0.00161 (@ 1064 nm)	0.89 (@ 1064 nm)	0.01017 (@ 880 nm) 0.01093 (@ 1050 nm)	4 (@ 1300 nm) 1.9 (@ 2100 nm)	∼90 (@ 895 nm)
Detectivity (Jones)	1.25×10^{12} (@ 850 nm) 6.65×10^{11} (@ 650 nm) 1.21×10^{12} (@ 1066 nm)	4.83×10^{9} (@ 1064 nm)	1.41×10^{11} (@ 1064 nm)	3.23×10^{10} (@ 880 nm) 3.47×10^{10} (@ 1050 nm)	——	——
EQE (%)	16090 (@ 850 nm) 10977 (@ 650 nm) 11552 (@ 1066 nm)	0.188 (@ 1064 nm)	103.58 (@ 1064 nm)	2.29 (@ 880 nm) 2.47 (@ 1050 nm)	——	——
Sensitivity	7.32 (@ 850 nm) 7.19 (@ 650 nm) 7.29 (@ 1066 nm)	.....	.....	4.32 (@ 880 nm) 5.74 (@ 1050 nm)	——–	——
Time Response (ON and OFF)	10.2 and 11.34 s (vis-NIR lamp)	8.6 and 1.9 s	5.8 and 4.5 s	5.99 and 13.58 s	——	0.3 and 1.7 s

and small exposed area of it. The carriers generated in graphene can freely follow both directions of the applied voltage since the work function of graphene and Ag are approximate equal [269, 270, 271] hence, the contact between Ag and graphene is ohmic (Fig.3.11) therefore, the carriers will not feel any barrier during the transportation for reverse as well as forward biasing. Due to large mobility of graphene this component of photo current is very fast.

The transportation of photo generated charge carriers in CTS QDs may happen in two manners, either the generated carriers in CTS QDs directly reach to the electrode

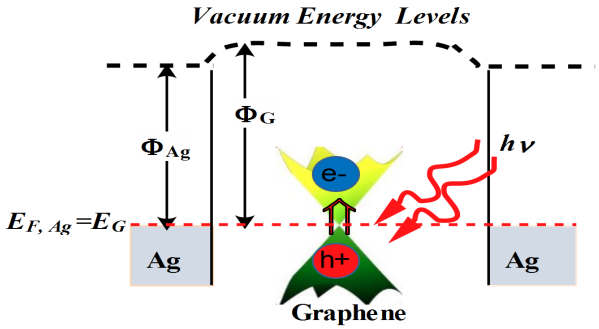

Figure 3.14: Band diagram of carriers transportation for Ag-Graphene-Ag component

and contribute the photo current (Ag-CTS QDs-Ag) or they may reach to electrode through the graphene layer (Ag-CTS QDs-Graphene-Ag). For both the mechanisms large photo current is achieved due to large carrier generation because of high surface to volume ratio of CTS QDs. The Ag-CTS QDs-Ag transport is sluggish in comparison to Ag-CTS QDs-Graphene-Ag due to high mobility of graphene.

Fig.3.15 represents the equivalent band diagram of Ag-Graphene-CTS QDs-Ag at thermal equilibrium (a) without any bias, (b) for forward bias and (c) for reverse bias. The work function of graphene, Ag and CTS QDs are denoted by ϕ_G, ϕ_{Ag}, and ϕ_{CTS}, respectively. While the electrons affinity and fermi level of CTS QDs are given by χ_{CTS} and $E_{F,CTS}$, respectively. $E_{V,CTS}$ and $E_{C,CTS}$ are the valence and conduction band energy levels of CTS QDs respectively. The contact between graphene and CTS is ohmic hence does not offer any resistance for the current flow in any direction i.e., under forward and reversed bias.

3.4 Conclusions

In this chapter, we have demonstrated a highly sensitive hybrid (0D/2D) broadband photodetector based CTS QDs and 2D-graphene to enhance the performance of only CTS QDs structure discussed in Chapter-2. The introduction of graphene with QDs structure has been done due to its high mobility and the ability to work as carrier transport layer for the generated photocarriers. The good quality CTS QDs have been synthesized using solvothermal method. CVD grown graphene is used to fabricate CTS

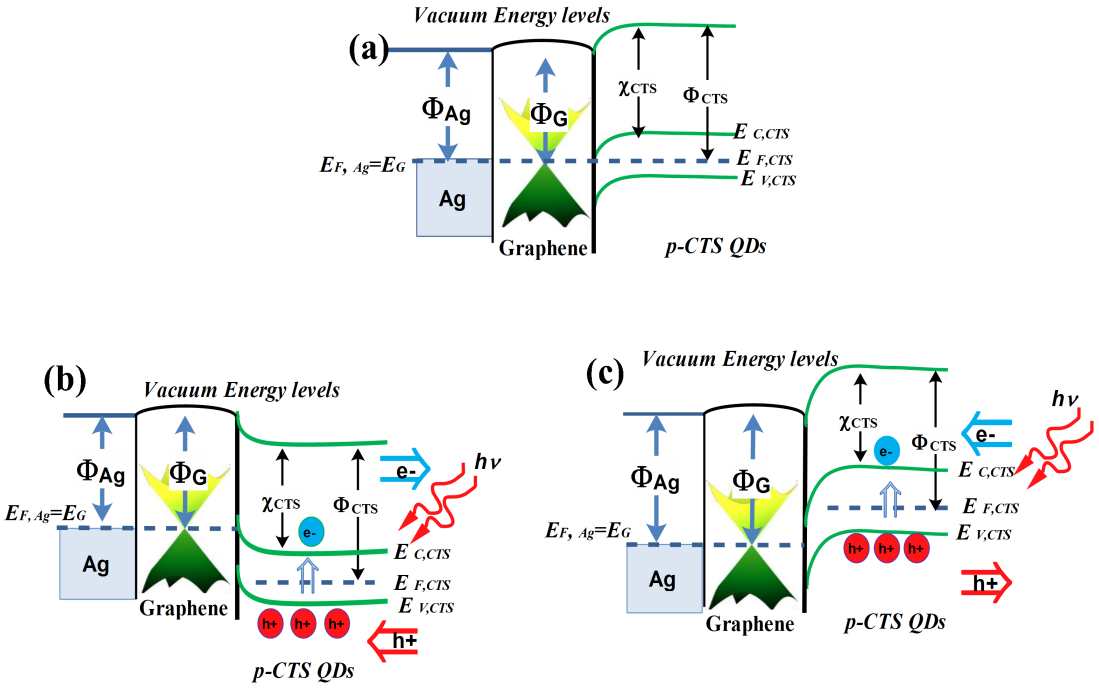

Figure 3.15: Energy band diagram of Ag/Graphene/CTS QDs hetero structures (a) Zero bias, (b) Forward bias, (c) Reverse bias.

QDs/Graphene hybrid photodetector structure. The device has almost flat response in spectrum region observed (vis-NIR) with highest responsivity and detectivity found ($\sim$110.089 A/W) and $\sim 1.25\times10^{12}$ (cm $\cdot Hz^{1/2} \cdot W^{-1}$) at 850 nm for 4.5 V bias. The time response of the proposed device is found to be comparable with the existing devices. The applications of the device may be found in optical communication, solar cell, in thermal imaging, remote sensing and in the field of bio-sensing.